Spontaneous gravity wave emission in in the differentially heated rotating annulus experiment

<u>Steffen Hien</u>, Joran Rolland & Ulrich Achatz
Institut für Atmospäre und Umwelt, Goethe Universität Frankfurt am Main

Sebastian Borchert
German Weather Service, Offenbach am Main

Lena Schoon & Christoph Zülicke
Leibniz-Institut für Atmosphärenphysik, University of Rostock

TRR 181 Workshop "Energy transfers in Atmosphere and Ocean", Hamburg 2017

IGW in the atmosphere

Internal gravity waves (IGW)

Orographic IGW

Nonorographic IGW

Convection

Jets/Fronts

"Spontaneous Emission"

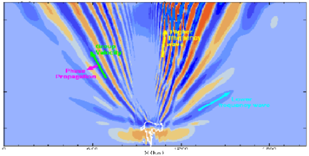

M. Joan Alexander - CEDAR Tutorial Lecture 06/21/02
(See Holton and Alexander (1999) for model description.)

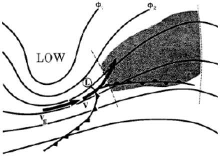

Koch and OHandley (1997)

IGW emission from jets and fronts

- IGW from jets and fronts contribute significantly to overall IGW spectrum (Plougonven and Zhang, 2014)

IGW emission from jets and fronts

- IGW from jets and fronts contribute significantly to overall IGW spectrum (Plougonven and Zhang, 2014)
- Physical understanding still insufficient to replace/improve existing, highly tuned parameterization schemes

IGW emission from jets and fronts

- IGW from jets and fronts contribute significantly to overall IGW spectrum (Plougonven and Zhang, 2014)
- Physical understanding still insufficient to replace/improve existing, highly tuned parameterization schemes
- Increasing desire to also incorporate climate sensitivity

IGW emission from jets and fronts

- IGW from jets and fronts contribute significantly to overall IGW spectrum (Plougonven and Zhang, 2014)
- Physical understanding still insufficient to replace/improve existing, highly tuned parameterization schemes
- Increasing desire to also incorporate climate sensitivity
- IGW signal embedded in various atmospheric processes ⇒ Extraction difficult

IGW emission from jets and fronts

- IGW from jets and fronts contribute significantly to overall IGW spectrum (Plougonven and Zhang, 2014)
- Physical understanding still insufficient to replace/improve existing, highly tuned parameterization schemes
- Increasing desire to also incorporate climate sensitivity
- IGW signal embedded in various atmospheric processes $\Rightarrow$ Extraction difficult
- Idealized dynamical systems facilitate investigations:
  - Baroclinically Unstable Flows (O'Sullivan and Dunkerton, 1995; Plougonven and Snyder, 2005)
  - Vortex dipole studies (Snyder et al., 2007; Wang et al., 2009)

IGW emission from jets and fronts

- IGW from jets and fronts contribute significantly to overall IGW spectrum (Plougonven and Zhang, 2014)
- Physical understanding still insufficient to replace/improve existing, highly tuned parameterization schemes
- Increasing desire to also incorporate climate sensitivity
- IGW signal embedded in various atmospheric processes ⇒ Extraction difficult
- Idealized dynamical systems facilitate investigations:
  - Baroclinically Unstable Flows (O'Sullivan and Dunkerton, 1995; Plougonven and Snyder, 2005)
  - Vortex dipole studies (Snyder et al., 2007; Wang et al., 2009)
- More freely generated jet-front system: **differentially heated rotating annulus experiment**

IGW emission from jets and fronts

- IGW from jets and fronts contribute significantly to overall IGW spectrum (Plougonven and Zhang, 2014)
- Physical understanding still insufficient to replace/improve existing, highly tuned parameterization schemes
- Increasing desire to also incorporate climate sensitivity
- IGW signal embedded in various atmospheric processes ⇒ Extraction difficult
- Idealized dynamical systems facilitate investigations:
  - Baroclinically Unstable Flows (O'Sullivan and Dunkerton, 1995; Plougonven and Snyder, 2005)
  - Vortex dipole studies (Snyder et al., 2007; Wang et al., 2009)
- More freely generated jet-front system: **differentially heated rotating annulus experiment**
- Possibility of comparison with corresponding laboratory studies

Differentially heated rotating annulus experiment

Simple laboratory experiment to reproduce dynamics of mid-latitudes

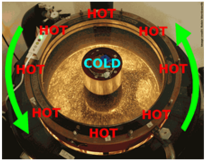

Laboratory experiment

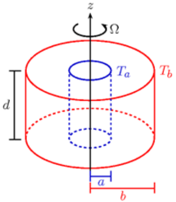

schematic view

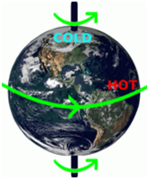

analogous to Earth's atmosphere

Differentially heated rotating annulus experiment

Simple laboratory experiment to reproduce dynamics of mid-latitudes

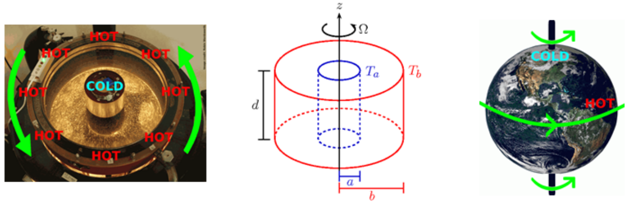

Laboratory experiment   schematic view   analogous to Earth's atmosphere

Parameter setting

- $a = 20\,\mathrm{cm},\ b = 70\,\mathrm{cm},\ d = 4\,\mathrm{cm}$

Differentially heated rotating annulus experiment

Simple laboratory experiment to reproduce dynamics of mid-latitudes

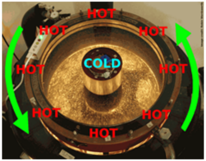

Laboratory experiment

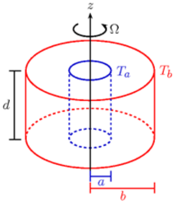

schematic view

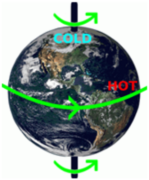

analogous to Earth's atmosphere

Parameter setting

- $a = 20\,\mathrm{cm},\ b = 70\,\mathrm{cm}, d = 4\,\mathrm{cm}$
- $T_a = 15°\mathrm{C},\ \ T_b = 45°\mathrm{C}$

Differentially heated rotating annulus experiment

Simple laboratory experiment to reproduce dynamics of mid-latitudes

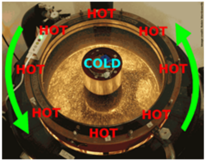

Laboratory experiment

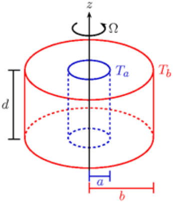

schematic view

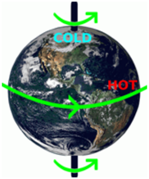

analogous to Earth's atmosphere

Parameter setting

- $a = 20\,\mathrm{cm},\ b = 70\,\mathrm{cm}, d = 4\,\mathrm{cm}$
- $T_a = 15^\circ\mathrm{C},\ \ T_b = 45^\circ\mathrm{C}$
- $\Omega = 0.08\,\mathrm{rad/s}$

Differentially heated rotating annulus experiment

Simple laboratory experiment to reproduce dynamics of mid-latitudes

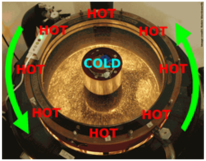

Laboratory experiment

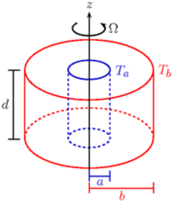

schematic view

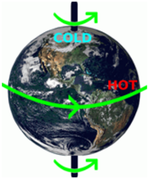

analogous to Earth's atmosphere

Parameter setting

- $a = 20\,\mathrm{cm},\ b = 70\,\mathrm{cm}, d = 4\,\mathrm{cm}$
- $T_a = 15°\mathrm{C},\ \ T_b = 45°\mathrm{C}$
- $\Omega = 0.08\,\mathrm{rad/s}$
- $\Rightarrow$ Atmosphere-like conditions

$$\frac{< N >}{f} > 1$$

Differentially heated rotating annulus experiment

Simple laboratory experiment to reproduce dynamics of mid-latitudes

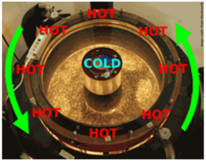

Laboratory experiment

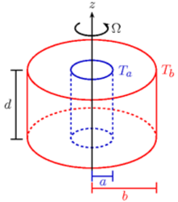

schematic view

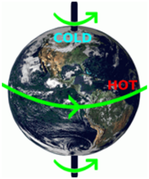

analogous to Earth's atmosphere

Parameter setting

- $a = 20\,\mathrm{cm},\ b = 70\,\mathrm{cm}, d = 4\,\mathrm{cm}$
- $T_a = 15°\mathrm{C},\ \ T_b = 45°\mathrm{C}$
- $\Omega = 0.08\,\mathrm{rad/s}$
- $\Rightarrow$ Atmosphere-like conditions

$$\frac{< N >}{f} > 1$$

Baroclinic waves (Borchert et al., 2015)

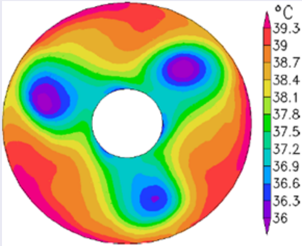

Direct numerical simulations: large-scale flow

- Clear baroclinic wave strucure including a jet-front system

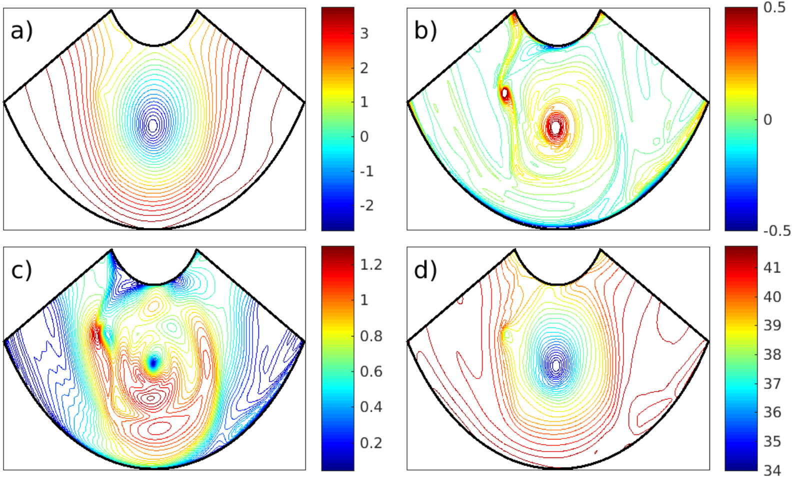

a) pressure, b) vertical vorticity, c) $||\boldsymbol{u}||$ and d) temperature

Direct numerical simulations: IGW activity

- Reduced horizontal velocity divergence δ used as IGW indicator

$$\delta = \underbrace{\delta_{total}}_{\boldsymbol{\nabla}_{\mathrm{h}}\cdot\boldsymbol{u}_{\mathrm{h}}} - \delta_{\mathrm{bal}},$$

where

$$\delta_{\mathrm{bal}} = -\frac{\partial w_{\mathrm{bal}}}{\partial z}\,.$$

Direct numerical simulations: IGW activity

- Reduced horizontal velocity divergence δ used as IGW indicator

$$\delta = \underbrace{\delta_{total}}_{\nabla_h \cdot \boldsymbol{u}_h} - \delta_{\mathrm{bal}},$$

where

$$\delta_{\mathrm{bal}} = -\frac{\partial w_{\mathrm{bal}}}{\partial z}\,.$$

- w_{bal} is diagnosed from the quasi-geostrophic omega equation (Hoskins et al. (1978), Danioux et al. (2012))

$$\nabla^2_{\mathrm{qg}} w_{\mathrm{bal}} = -\frac{2}{N^2} \boldsymbol{\nabla}_{\mathrm{h}} \cdot \boldsymbol{Q},$$

where

$$\boldsymbol{Q} = \boldsymbol{\nabla}_{\mathrm{h}} \boldsymbol{u}_{\mathbf{g}} \cdot \boldsymbol{\nabla}_{\mathrm{h}} B_{\mathrm{g}}\,.$$

only depends on quasi-geostrophic fields.

Balanced and unbalanced flow and their interaction

Diagnosing balanced part in horizontal divergence: omega equation

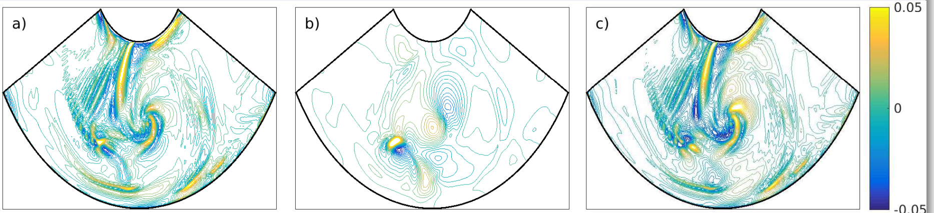

δ_{total} δ_{bal} δ_{unbal}

- Four distinct wave packets **(WP1 – WP4)** can be identified
  (Hien et al., submitted)

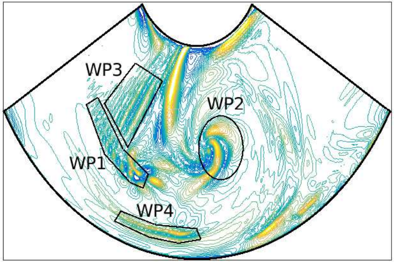

Annulus geometry

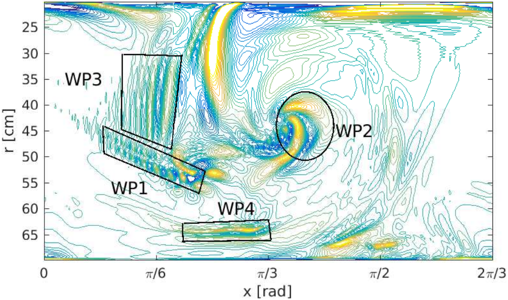

Cartesian projection

Direct numerical simulations: IGW activity

- Wave packet analysis ($\boldsymbol{k}$, $\boldsymbol{A}$,..) using **UWaDi (Unified Wave Diagnostics)** based on Hilbert-transform algorithm
- Reference for related laboratory studies

Direct numerical simulations: IGW activity

- Wave packet analysis (***k***, ***A***,..) using **UWaDi (Unified Wave Diagnostics)** based on Hilbert-transform algorithm
- Reference for related laboratory studies

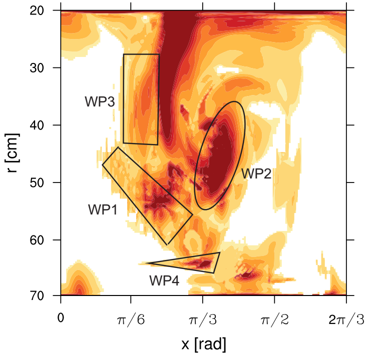

Amplitudes [1/s]

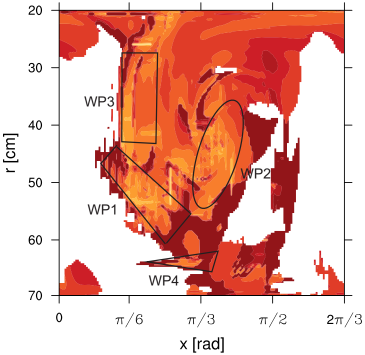

wave numbers [1/cm]

Balanced and unbalanced flow and their interaction

Decomposition of flow into geostrophic and ageostrophic part

$$
\begin{aligned}
\boldsymbol{v} &= \boldsymbol{u}_{\mathrm{g}} + \boldsymbol{v}_{\mathrm{a}} \\
B &= B_{\mathrm{g}} + B_{\mathrm{a}} \\
p &= p_{\mathrm{g}} + p_{\mathrm{a}}
\end{aligned}
$$

Balanced and unbalanced flow and their interaction

Decomposition of flow into geostrophic and ageostrophic part

$$
\begin{aligned}
\boldsymbol{v} &= \boldsymbol{u}_\mathrm{g} + \boldsymbol{v}_\mathrm{a} \\
B &= B_\mathrm{g} + B_\mathrm{a} \\
p &= p_\mathrm{g} + p_\mathrm{a}
\end{aligned}
$$

$$
\begin{aligned}
f \mathbf{e_z} \times \boldsymbol{u}_\mathbf{g} + \nabla_h p_\mathrm{g} &= 0 \\
B_\mathrm{g} - \frac{\partial p_\mathrm{g}}{\partial z} &= 0 \\
\Pi_\mathrm{g} = \zeta + \frac{f}{N^2}\frac{\partial B}{\partial z} &= \frac{1}{f}\left(\nabla_h^2 + \frac{f^2}{N^2}\frac{\partial^2}{\partial z^2}\right) p_\mathrm{g} \\
\zeta_\mathrm{a} + \frac{f}{N^2}\frac{\partial B_\mathrm{a}}{\partial z} &= 0
\end{aligned}
$$

Balanced and unbalanced flow and their interaction

Decomposition of flow into geostrophic and ageostrophic part

$$\begin{aligned} \mathbf{v} &= \mathbf{u}_g + \mathbf{v}_a \\ B &= B_g + B_a \\ p &= p_g + p_a \end{aligned}$$

$$\begin{aligned} f\mathbf{e_z} \times \mathbf{u_g} + \nabla_h p_g &= 0 \\ B_g - \frac{\partial p_g}{\partial z} &= 0 \\ \Pi_g = \zeta + \frac{f}{N^2}\frac{\partial B}{\partial z} &= \frac{1}{f}\left(\nabla_h^2 + \frac{f^2}{N^2}\frac{\partial^2}{\partial z^2}\right) p_g \\ \zeta_a + \frac{f}{N^2}\frac{\partial B_a}{\partial z} &= 0 \end{aligned}$$

... ⇒ Geostrophic forcing of ageostrophic flow

$$\frac{D\delta_a}{Dt} = -\frac{\partial B_a}{\partial z} + \frac{\partial^2 p_{aa}}{\partial z^2} + \frac{\partial \mathbf{v}}{\partial z} \cdot \nabla w_a - \boxed{\frac{\partial^2}{\partial z^2}\nabla^{-2}\left(\nabla \mathbf{u_g} \cdot \cdot \nabla \mathbf{u_g}\right)}$$

Source mechanism of IGWs

Tangent linear model for the ageostrophic flow: Principle

- Decomposition into balanced (large) and unbalanced (small) part

$$\boldsymbol{x} = \tilde{\boldsymbol{x}} + \boldsymbol{x}' \text{ with } |\boldsymbol{x}'| \ll |\tilde{\boldsymbol{x}}| \quad (\textbf{Unbalanced part} \approx \textbf{gravity waves})$$

Tangent linear model for the ageostrophic flow: Principle

- Decomposition into balanced (large) and unbalanced (small) part

$$\boldsymbol{x} = \tilde{\boldsymbol{x}} + \boldsymbol{x}' \text{ with } |\boldsymbol{x}'| \ll |\tilde{\boldsymbol{x}}| \quad (\textbf{Unbalanced part} \approx \textbf{gravity waves})$$

- Inserting this into the full equation system gives

$$\frac{\partial \boldsymbol{x}}{\partial t} = \frac{\partial \tilde{\boldsymbol{x}}}{\partial t} + \frac{\partial \boldsymbol{x}'}{\partial t} = \boldsymbol{N}(\boldsymbol{x}),$$

where $\boldsymbol{N}(\boldsymbol{x})$ is the nonlinear tendency of the full flow.

Source mechanism of IGWs

Tangent linear model for the ageostrophic flow: Principle

- Decomposition into balanced (large) and unbalanced (small) part

$$\boldsymbol{x} = \tilde{\boldsymbol{x}} + \boldsymbol{x}' \text{ with } |\boldsymbol{x}'| \ll |\tilde{\boldsymbol{x}}| \;\; (\textbf{Unbalanced part} \approx \textbf{gravity waves})$$

- Inserting this into the full equation system gives

$$\frac{\partial \boldsymbol{x}}{\partial t} = \frac{\partial \tilde{\boldsymbol{x}}}{\partial t} + \frac{\partial \boldsymbol{x}'}{\partial t} = \boldsymbol{N}(\boldsymbol{x}),$$

  where $\boldsymbol{N}(\boldsymbol{x})$ is the nonlinear tendency of the full flow.

- Taylor approximation leads to

$$\boldsymbol{N}(\tilde{\boldsymbol{x}} + \boldsymbol{x}') = \boldsymbol{N}(\tilde{\boldsymbol{x}}) + \boldsymbol{L}(\tilde{\boldsymbol{x}})\boldsymbol{x}' + \mathcal{O}(|\boldsymbol{x}'|^2)$$

  with the linear, partial-differential operator $\boldsymbol{L}(\tilde{\boldsymbol{x}})\boldsymbol{x}'$

Source mechanism of IGWs

Tangent linear model for the ageostrophic flow: Principle

- Hence, the tangent linear evolution of $\boldsymbol{x'}$ is given by

$$\frac{\partial \boldsymbol{x'}}{\partial t} = L(\tilde{\boldsymbol{x}})\boldsymbol{x'} + \underbrace{\boldsymbol{N}(\tilde{\boldsymbol{x}}) - \frac{\partial \tilde{x}}{\partial t}}_{\boldsymbol{F}(\tilde{x})}$$

  with a balanced forcing term $F(\tilde{\boldsymbol{x}})$.

Source mechanism of IGWs

Tangent linear model for the ageostrophic flow: Principle

- Hence, the tangent linear evolution of $\boldsymbol{x'}$ is given by

$$\frac{\partial \boldsymbol{x'}}{\partial t} = L(\tilde{\boldsymbol{x}})\boldsymbol{x'} + \underbrace{\boldsymbol{N}(\tilde{\boldsymbol{x}}) - \frac{\partial \tilde{x}}{\partial t}}_{\boldsymbol{F}(\tilde{x})}$$

  with a balanced forcing term $F(\tilde{\boldsymbol{x}})$.

- Implementation of window function to suppress instabilities and IGW generation at side walls

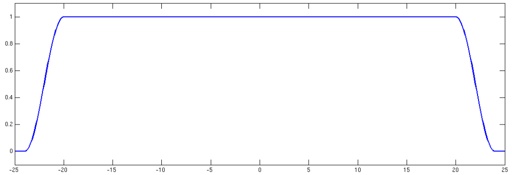

Source mechanism of IGW: Tangent linear analysis

Tangent linear annulus equation

$$\frac{\mathrm{D}\boldsymbol{u}_{\mathbf{a}}}{\mathrm{Dt}} = -f\,\boldsymbol{e}_{\mathbf{z}} \times \boldsymbol{u}_{\mathbf{a}} - \nabla_h \tilde{p}_{\mathrm{a}} - \left(\frac{\mathrm{D}\boldsymbol{u}_{\mathbf{g}}}{\mathrm{Dt}}\right)_{\mathrm{a}} - \left\{\left(\frac{\mathrm{D}\boldsymbol{u}_{\mathbf{g}}}{\mathrm{Dt}}\right)_{\mathrm{g}}\right\}$$

$$\frac{\mathrm{D}B_{\mathrm{a}}}{\mathrm{Dt}} = -N^2 w_{\mathrm{a}} - \left(\frac{\mathrm{D}B_{\mathrm{g}}}{\mathrm{Dt}}\right)_{\mathrm{a}} - \left\{\left(\frac{\mathrm{D}B_{\mathrm{g}}}{\mathrm{Dt}}\right)_{\mathrm{g}}\right\}$$

$$\frac{\mathrm{D}w_{\mathrm{a}}}{\mathrm{Dt}} = B_{\mathrm{a}} - \frac{\partial \tilde{p}_{\mathrm{a}}}{\partial z}$$

Source mechanism of IGW: Tangent linear analysis

Tangent linear annulus equation

$$\frac{\mathrm{D}\boldsymbol{u}_\mathrm{a}}{\mathrm{D}t} = -f\,\boldsymbol{e}_\mathbf{z}\times\boldsymbol{u}_\mathrm{a} - \nabla_h\tilde{p}_\mathrm{a} - \left(\frac{\mathrm{D}\boldsymbol{u}_\mathbf{g}}{\mathrm{D}t}\right)_\mathrm{a} - \left\{\left(\frac{\mathrm{D}\boldsymbol{u}_\mathbf{g}}{\mathrm{D}t}\right)_\mathrm{g}\right\}$$

$$\frac{\mathrm{D}B_\mathrm{a}}{\mathrm{D}t} = -N^2 w_\mathrm{a} - \left(\frac{\mathrm{D}B_\mathrm{g}}{\mathrm{D}t}\right)_\mathrm{a} - \left\{\left(\frac{\mathrm{D}B_\mathrm{g}}{\mathrm{D}t}\right)_\mathrm{g}\right\}$$

$$\frac{\mathrm{D}w_\mathrm{a}}{\mathrm{D}t} = B_\mathrm{a} - \frac{\partial\tilde{p}_\mathrm{a}}{\partial z}$$

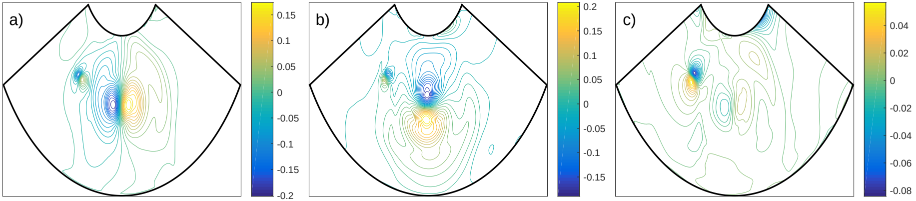

forcing of u_a forcing of v_a forcing of B_a

Sources of IGW in the rotating annulus experiment

Initialisation of linear model with zero ageostrophic part at $t = 0\,\mathrm{s}$

Sources of IGW in the rotating annulus experiment

Initialisation of linear model with zero ageostrophic part at $t = 0\,\mathrm{s}$

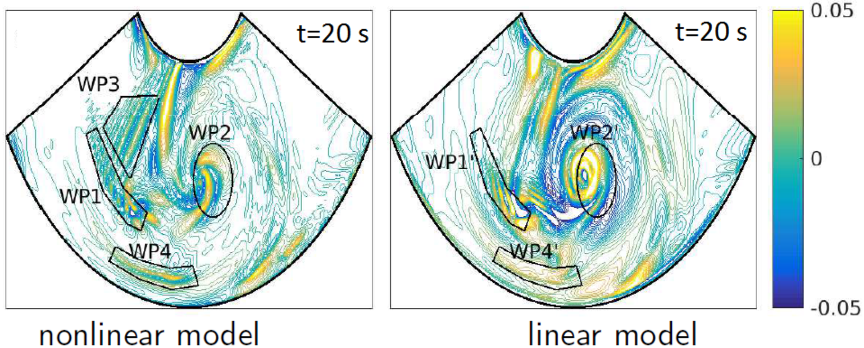

Sources of IGW in the rotating annulus experiment

Initialisation of linear model with zero ageostrophic part at $t = 0\,\mathrm{s}$

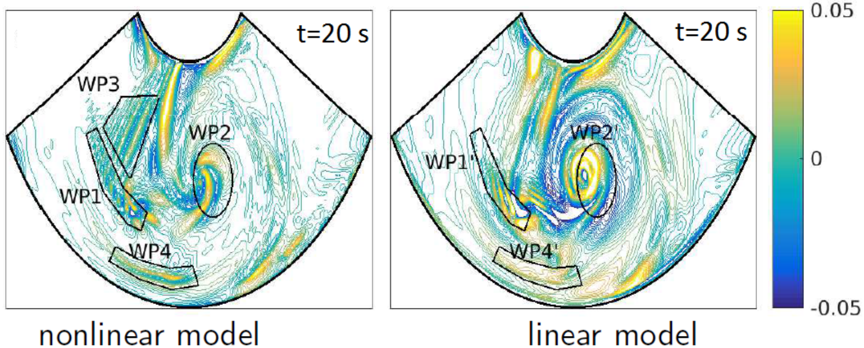

- WP1, WP2 and WP4 reproduced by linear model, WP3 is not present

Sources of IGW in the rotating annulus experiment

Initialisation of linear model with zero ageostrophic part at $t = 0\,\mathrm{s}$

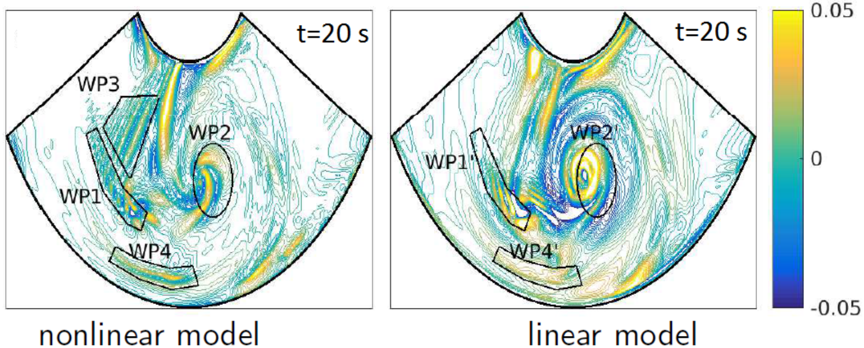

- WP1, WP2 and WP4 reproduced by linear model, WP3 is not present
- At t=0 s, (only) balanced forcing induces ageostrophic flow (and IGWs)

Sources of IGW in the rotating annulus experiment

Initialisation of linear model with zero ageostrophic part at $t = 0\,\mathrm{s}$

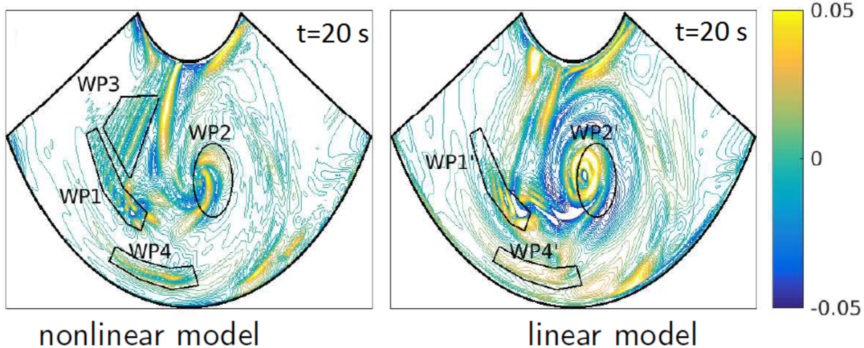

- WP1, WP2 and WP4 reproduced by linear model, WP3 is not present
- At t=0 s, (only) balanced forcing induces ageostrophic flow (and IGWs) $\Rightarrow$ WP1, WP2 and WP4 emitted by balanced part of the flow

Sources of IGW in the rotating annulus experiment

Initialisation of linear model with zero ageostrophic part at $t = 0\,\mathrm{s}$

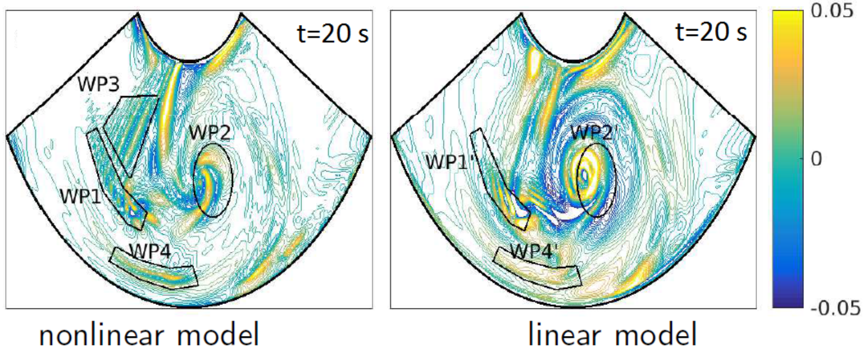

- WP1, WP2 and WP4 reproduced by linear model, WP3 is not present
- At t=0 s, (only) balanced forcing induces ageostrophic flow (and IGWs) $\Rightarrow$ WP1, WP2 and WP4 emitted by balanced part of the flow
- WP3 is probably generated at inner side wall

(for details see Jacoby et al. (2011); Randriamampianina and Crespo del Arco (2015))

Sources of IGW and role of balanced forcing

Initialisation of linear model with non-zero ageostrophic part

- Three model configurations: Fully nonlinear, forced linear and unforced linear ($F = 0$)

Sources of IGW and role of balanced forcing

Initialisation of linear model with non-zero ageostrophic part

- Three model configurations: Fully nonlinear, forced linear and unforced linear ($F = 0$)
- Initialisation with same (non-zero) ageostrophic field at $t \equiv 0\,\mathrm{s}$

Sources of IGW and role of balanced forcing

Initialisation of linear model with non-zero ageostrophic part

- Three model configurations: Fully nonlinear, forced linear and unforced linear ($F = 0$)
- Initialisation with same (non-zero) ageostrophic field at $t \equiv 0\,\mathrm{s}$

$$\boldsymbol{x}' = \boldsymbol{x} - \tilde{\boldsymbol{x}}$$

Sources of IGW and role of balanced forcing

Initialisation of linear model with non-zero ageostrophic part

- Three model configurations: Fully nonlinear, forced linear and unforced linear ($F = 0$)
- Initialisation with same (non-zero) ageostrophic field at $t \equiv 0\,\mathrm{s}$

$$\boldsymbol{x}' = \boldsymbol{x} - \tilde{\boldsymbol{x}}$$

- Wave packets already present at initial time t=0 s

Initialisation of linear model with non-zero ageostrophic part

- Three model configurations: Fully nonlinear, forced linear and unforced linear ($F = 0$)
- Initialisation with same (non-zero) ageostrophic field at $t \equiv 0\,\mathrm{s}$

$$\boldsymbol{x}' = \boldsymbol{x} - \tilde{\boldsymbol{x}}$$

- Wave packets already present at initial time t=0 s

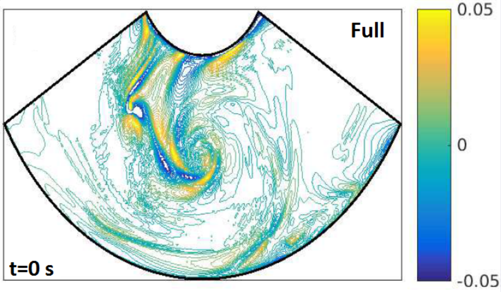

Sources of IGW and role of balanced forcing

Initialisation of linear model with non-zero ageostrophic part

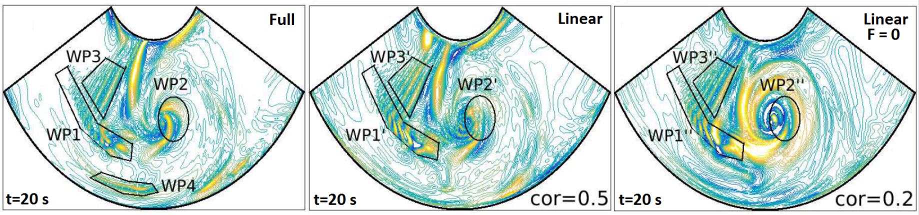

Sources of IGW and role of balanced forcing

Initialisation of linear model with non-zero ageostrophic part

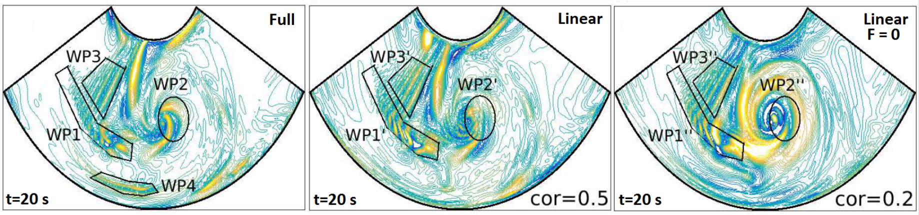

- Balanced forcing controls over structure around vortex dipole

Sources of IGW and role of balanced forcing

Initialisation of linear model with non-zero ageostrophic part

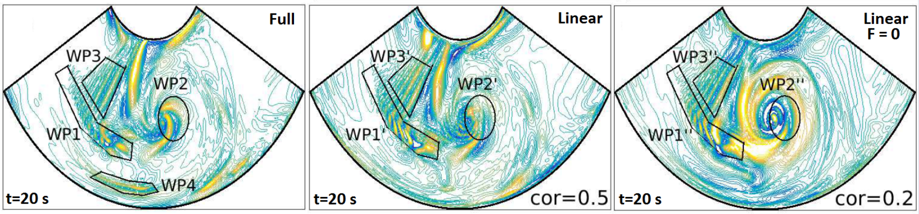

- Balanced forcing controls over structure around vortex dipole
- Propagation of WP1 and WP3 captured by linear models ⇒ Forcing controls over generation but only minor on propagation

Sources of IGW and role of balanced forcing

Initialisation of linear model with non-zero ageostrophic part

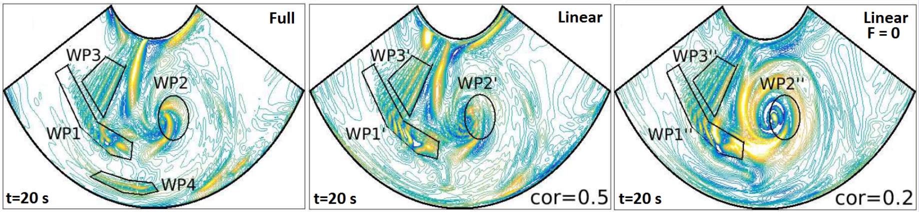

- Balanced forcing controls over structure around vortex dipole
- Propagation of WP1 and WP3 captured by linear models ⇒ Forcing controls over generation but only minor on propagation
- WP2 differs significantly in unforced linear model ⇒ WP2 is continuously affected by internal forcing

Initialisation of linear model with non-zero ageostrophic part

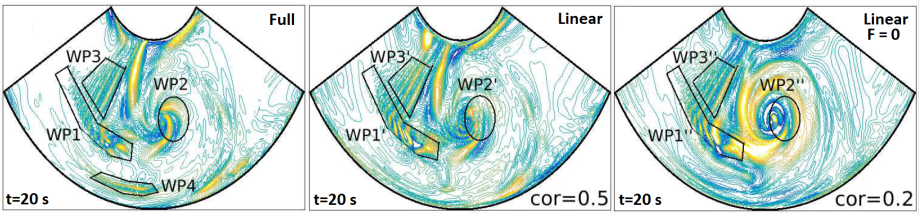

- Balanced forcing controls over structure around vortex dipole
- Propagation of WP1 and WP3 captured by linear models ⇒ Forcing controls over generation but only minor on propagation
- WP2 differs significantly in unforced linear model ⇒ WP2 is continuously affected by internal forcing
- WP4 only hardly identifiable ⇒ effect of window function?

Sources of IGW and role of balanced forcing

Time evolution of 3D correlation coefficient between (un)forced linear and nonlinear model

- Only grid points not affected by window function are taken into account

Sources of IGW and role of balanced forcing

Time evolution of 3D correlation coefficient between (un)forced linear and nonlinear model

- Only grid points not affected by window function are taken into account

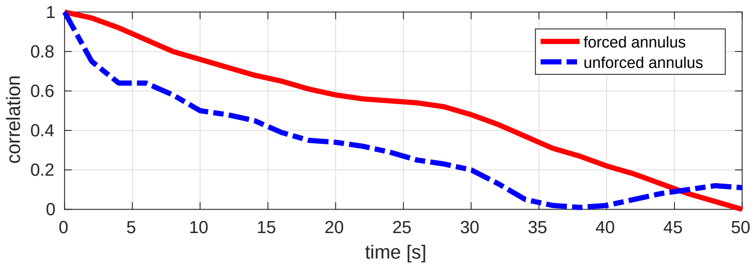

Conclusions

Conclusions

- Numerical simulations of differentially heated rotating annulus experiment show baroclinic wave structure exhibiting a realistic jet-front system.

Conclusions

- Numerical simulations of differentially heated rotating annulus experiment show baroclinic wave structure exhibiting a realistic jet-front system.
- IGWs occur in four distinct wave packets. Characterization with UWaDi.

Conclusions

- Numerical simulations of differentially heated rotating annulus experiment show baroclinic wave structure exhibiting a realistic jet-front system.
- IGWs occur in four distinct wave packets. Characterization with UWaDi.
- Tangent linear analysis indicates that significant part of IGWs originate from jet-front system: spontaneous emission of IGWs by internal flow (Zhang, 2004)

Conclusions

Conclusions

- Numerical simulations of differentially heated rotating annulus experiment show baroclinic wave structure exhibiting a realistic jet-front system.
- IGWs occur in four distinct wave packets. Characterization with UWaDi.
- Tangent linear analysis indicates that significant part of IGWs originate from jet-front system: spontaneous emission of IGWs by internal flow (Zhang, 2004) .

Outlook

- Investigation of IGW radiation by jets and fronts in ever more realistic flow configurations

Conclusions

Conclusions

- Numerical simulations of differentially heated rotating annulus experiment show baroclinic wave structure exhibiting a realistic jet-front system.
- IGWs occur in four distinct wave packets. Characterization with UWaDi.
- Tangent linear analysis indicates that significant part of IGWs originate from jet-front system: spontaneous emission of IGWs by internal flow (Zhang, 2004) .

Outlook

- Investigation of IGW radiation by jets and fronts in ever more realistic flow configurations
- ...
- Physically based source parameterization of IGWs in large-scale background flow

References

Borchert, S., U. Achatz, S. Remmler, S. Hickel, U. Harlander, M. Vincze, K. Alexandrov, F. Rieper, T. Heppelmann, and S. Dolaptchiev. (2015). Finite-volume models with implicit subgrid-scale parameterization for the differentially heated rotating annulus. *Meteorol. Z. 23*(6), 561–580.

Danioux, E., J. Vanneste, P. Klein, and H. Sasaki. (2012). Spontaneous inertia-gravity-wave generation by surface-intensified turbulence. *J. Fluid Mech. 699*, 153–173.

Hoskins, B., I. Draghici, and H. Davies (1978). A new look at the omega-equation. *Q. J. R. Meteorol. Sci. 104*, 31–38.

Jacoby, T. N. L., P. L. Read, P. D. Williams, and R. M. B. Young (2011). Generation of inertia-gravity waves in the rotating thermal annulus by a localised boundary layer instability. *Geophys. Astrophys. Fluid Dyn. 105*, 161–181.

O'Sullivan, D. and T. J. Dunkerton (1995). Generation of inertia-gravity waves in a simulated life cycle of baroclinic instability. *J. Atmos. Sci. 52*, 3695–3716.

Plougonven, R. and C. Snyder (2005). Gravity waves excited by jets: propagation versus generation. *Geophys. Res. Lett. 32*, L18802.

Plougonven, R. and F. Zhang (2014). Internal gravity waves from atmospheric jets and fronts. *Rev. Geophys. 52*(1), 33–76.

Randriamampianina, A. and E. Crespo del Arco (2015). Inertia-gravity waves in a liquid-filled, differentially heated, rotating annulus. *J. Fluid Mech. 782*, 144–177.

Snyder, C., D. J. Muraki, R. Plougonven, and F. Zhang (2007). Inertia-gravity waves generated within a dipole vortex. *J. Atmos. Sci. 64*, 4417–4431.

Wang, S., F. Zhang, and C. Snyder (2009). Generation and propagation of inertia-gravity waves from vortex dipoles and jets. *J. Atmos. Sci. 66*, 1294–1314.

Zhang, F. (2004). Generation of mesoscale gravity waves in upper-tropospheric jet–front systems. *J. Atmos. Sci. 61*, 440–457.